ELSEVIER

Journal of Magnetism and Magnetic Materials 239 (2002) 224–227

Journal of magnetism and magnetic materials

www.elsevier.com/locate/jmmm

Vertical self-organization of epitaxial magnetic nanostructures

O. Fruchart[a,b,*], P.-O. Jubert[a], C. Meyer[a], M. Klaua[b], J. Barthel[b], J. Kirschner[b]

[a] *Laboratoire Louis Néel (CNRS), BP166, F-38042 Grenoble, Cedex 9, France*
[b] *MPI für Mikrostrukturphysik, Weinberg 2, D-06120 Halle, Germany*

Abstract

We report the fabrication of epitaxial nanometer-thick magnetic structures, self-organized on surface reconstructions [Co/Au (1 1 1) pillars] and atomic step arrays [Fe/Mo (1 1 0) stripes]. Due to their high volume, these structures are remanent at room temperature, whereas conventional self-organized flat systems obtained in the sub-monolayer deposition range are superparamagnetic down to low temperatures.

Keywords: Self-organization; Epitaxial growth; Superparamagnetism; Surface reconstruction, Atomic step

1. Introduction

During the last decade, it has been shown that nanostructures can be fabricated spontaneously during ultra-high vacuum (UHV) deposition of a fraction of, or a few atomic layers. Although generally randomly distributed, in a few cases the nanostructures can be forced to nucleate in a well-ordered fashion when deposited on a patterned template surface. The successful use of several types of templates was reported for magnetic deposits, such as arrays of atomic steps on vicinal surfaces [1,2], arrays of overlayer [3] or buried [4] dislocations, medium range intrinsic [5] or adsorbate-driven [6] surface reconstructions. These processes are often called self-organization.

Until now very few studies have been reported on the magnetic properties of these systems, which remain in the field of fundamental surface physics. One reason is that self-organized magnetic systems are considered as limited in number and not versatile. Another reason is that these nanostructures are generally so small and thin that they are superparamagnetic or even nonmagnetic at room temperature. Here, we describe two attempts to overcome these obstacles, based on self-organization on surface reconstructions and atomic steps, successively. It is shown how manipulation of growth can bring these systems from surface physics to material physics by increasing their size perpendicular to the surface, while retaining their initial in-plane shape and order.

2. Vertical CO/AU (1 1 1) pillars

The Au (1 1 1) surface is unique: it undergoes a surface reconstruction whose lattice parameters are well above the atomic dimensions: $\sim 7.5 \times 20$ nm. This template has been used in the sub-atomic-layer range to fabricate self-organized arrays of flat Co, Ni and Fe dots with diameter in the range 1–5 nm and density above 10^{12} cm^{-2} (see left part of Fig. 1) [7–9]. Fe and Ni dots are 1 atomic layer (AL) high, whereas Co dots are 2 AL high, and all dots are superparamagnetic above 10–30 K. We reported recently that the flat Co dots could be extended vertically by sequential deposition of subAL amounts of Au and Co under suitable conditions. Firstly, Au atoms fill the empty space between Co dots and smooth the surface. Then during Co deposition Co atoms gather on top of existing Co dots, heightening them by 1 AL. Self-organized arrays of vertical Co pillars are obtained by repetition of many similar steps [10,11] (see right part of Fig. 1). Magnetization is perpendicular to the surface, and the blocking temperature is higher than in conventional flat dots due to the increased number of Co atoms per magnetic entity. To

*Corresponding author. Tel.: +33-76-887920; fax: +33-76-881191.
E-mail address: fruch@polycnrs-gre.fr (O. Fruchart).

0304-8853/02/$ - see front matter
PII: S0304-8853(01)00533-9

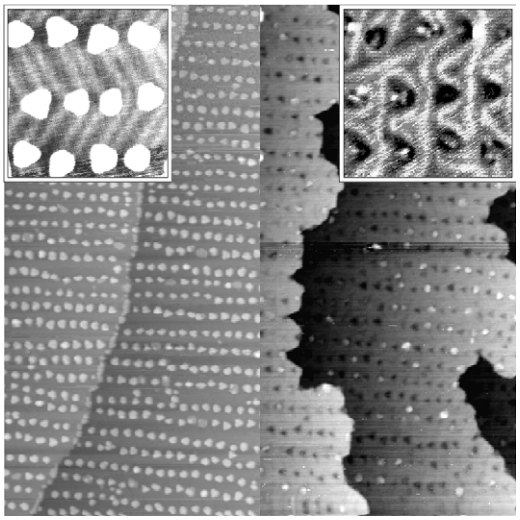

Fig. 1. 300×300 nm STM image of self-organized Co/Au (1 1 1) dots in the monolayer range (left) and after deposition of 10 Co/Au bilayers (right, different area). Insets show enlargements with the Au reconstruction clearly visible.

some extent, the diameter and the height of the pillars can be tuned by the fraction of AL of Co deposited during each step, and the total number of steps, respectively, while the lateral spacing is kept fixed, as imposed by the Au (1 1 1) reconstruction. It is the purpose of this section to report how magnetic properties of such pillars depend on their geometry. We report on four samples labeled A–D, whose geometrical features are summarized in Table 1, along with magnetic properties to be discussed below.

Fig. 2 shows the normalized polar magneto-optical Kerr effect hysteresis loops of samples A–D measured in situ up to 0.75 T, from 60 to 300 K. Remanence is weak in all samples resulting from both thermal activation and inter-pillar demagnetizing fields, as argued below.

Concerning thermal activation it is clear that the blocking temperature T_B increases with the mean pillar volume, from 80 K in A to above 300 K in D. We first focus on the superparamagnetic regime of pillars in A, ranging from 80 to 300 K. Our discussion below gives a firmer basis to what had already been partly disclosed in Ref. [11] concerning the analysis of the superparamagnetic regime. Although each pillar holds a macroscopic spin the Langevin function cannot be used to fit the $M(H,T)$ response because of the nonzero magnetic anisotropy. Let us consider a pillar of energy $E = -\mu_0 MH\cos\theta - K\cos^2\theta$. $M = M_s v$ and $K = K_v v$ where M_s and K_v are respectively, the saturation magnetization and anisotropy per unit volume, v is the pillar volume, and θ is the angle between the magnetization vector and the normal to the film. We also assume as a crude

Table 1
Features of samples A–D

Pillars in sample	Diameter (nm)	Height (nm)	Volume (nm^3)	T_B (K)
A	3	5.5	40	80
B	4.3	4.5	65	210
C	4.2	8	110	300
D	3.9	18	215	350

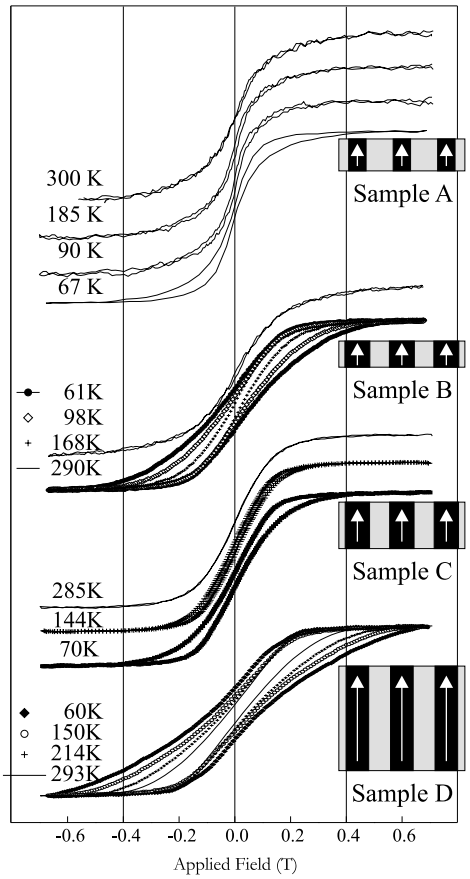

Fig. 2. Polar MOKE hysteresis loops of samples A–D. Note that sample D could not be saturated under 0.75 T below 125 K, so that the displayed loops are minor loops.

approximation that the pillar macrospin follows the Boltzmann law at equilibrium. The partition function of the pillar can be calculated exactly:

$$Z = (\sqrt{\pi}/2\sqrt{d})\exp(-h^2/4d) \times \left[\mathrm{Erfi}(\sqrt{d} + h/2\sqrt{d}) + \mathrm{Erfi}(\sqrt{d} - h/2\sqrt{d})\right] \quad (1)$$

with $d = \beta K$, $h = \beta\mu_0 MH$, $\beta = 1/k_B T$ and $\mathrm{Erfi}(x) = (2/\sqrt{\pi})\int_0^x e^{t^2}\mathrm{d}t$ is the imaginary error function. It is then straightforward to derive the average normalized magnetization $x = \cos\theta$:

$$x = -h/2d + (2/\sqrt{\pi d}) \times \frac{\exp(d + h^2/4d)\sinh(h)}{\mathrm{Erfi}(\sqrt{d} + h/2\sqrt{d}) + \mathrm{Erfi}(\sqrt{d} - h/2\sqrt{d})}, \quad (2)$$

as well as the initial susceptibility $\xi = \mathrm{d}x/\mathrm{d}h$:

$$\xi = -1/2d + \exp(d)/(\sqrt{\pi d}\,\mathrm{Erfi}\,\sqrt{d}). \quad (3)$$

These analytical expressions valid over the entire field range extend the initial susceptibility calculations of Ref. [12]. In the high temperature/low anisotropy limit Eq. (2) comes close to the Langevin function, and $\xi \sim 1/3 + 4d/45$. In this limit thermal activation becomes so high that all macrospin directions are nearly equally probable. Numerical evaluation shows that this approximation is very good for $T > 50\,T_B$, with $T_B \sim K/25k_B$. In the low temperature/high anisotropy limit Eq. (2) comes close to the Brillouin $\frac{1}{2}$ function, and $\xi \sim 1 - 1/d$. This approximation is very good for $T < 5\,T_B$, which is the case for sample A. This can be understood as follows. Even being above T_B the macrospin remains most of the time not far from an easy axis direction for $T < 5T_B$, either up or down, and only very rare events allow magnetization to switch in the time scale of measurement, typically 1 s. Finally, as in Ref. [11], H includes the external field, plus inter-pillar dipolar fields estimated in a mean field approach: $H = H_{ext} + \alpha M_s(m/M)$ with $m = M\cos\theta$, where α is a geometrical factor. The reverse initial normalized susceptibility is then given by

$$\frac{1}{\chi} = M\frac{\mathrm{d}(\mu_0 H)}{\mathrm{d}m} = \frac{k_B T}{M}\left(1 + \frac{k_B T}{K}\right) - \alpha(\mu_0 M_s). \quad (4)$$

The experimental $1/\chi(T)$ curve is linear within experimental error (see Fig. 3b), which shows that the pertubation term $k_B T/K$ in Eq. (4) can be neglected in our case. The intercept with the y-axis yields $\alpha(\mu_0 M_s) = -42\,\mathrm{mT}$, and the slope yields $N = 2800$ Co atoms per pillar. These figures are in good agreement with those estimated from the geometry of the pillars deduced by STM: $\alpha(\mu_0 M_s) = -32\,\mathrm{mT}$ and $N = 3300$ atoms. This good agreement confirms the continuity of the pillars which had been suggested in the view of STM images, and suggests that each pillar behaves like a single magnetic entity [11]. For samples B–D the agreement over α is also quantitatively good, but N (proportional to M/M_s) cannot be reliably estimated because in Eq. (4) the term $\alpha(\mu_0 M_s)$ is dominant. Finally, note that $\alpha < 0$ means that inter-pillar dipolar fields are demagnetizing as expected from neighboring spins with perpendicular anisotropy. This might also explain why the remanent magnetization remains moderate below T_B despite the perpendicular anisotropy.

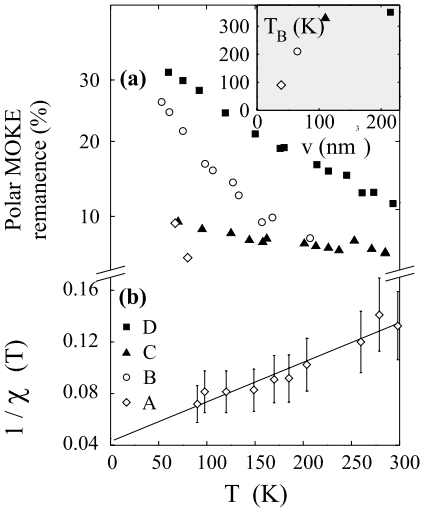

Fig. 3. (a) Polar remanence for samples A–D (b) Inverse susceptibility of sample A.

Fig. 3a shows the normalized remanent magnetization M_r of samples A–D as a function of temperature. From these curves, we estimated T_B for each sample by measuring or extrapolating the cancellation temperature of M_r. T_B is found to increase with the mean pillar volume v (see inset), with a tendency towards saturation for large pillars. As the anisotropy barrier preventing magnetization reversal is $K = K_v v$, this suggests that the effective magnetic anisotropy per unit volume K_v is only weakly dependent on the pillar size and geometry.

Let us finally comment on the moderate increase of M_r below T_B, whereas a sharp rise is expected for a single domain isolated superparamagnetic pillar. One reason for a moderate M_r just below T_B is demagnetizing inter-pillar dipolar fields. This is confirmed by the fact that remanence is lower in samples A and C than in samples B and D, which is correlated to the fact that the lateral order of the pillars is more altered during the course of vertical growth in samples B and D (to be reported elsewhere), yielding weaker inter-pillar demagnetizing fields. However, M_r should in both cases dramatically increase towards 1 well below T_B, as the demagnetizing fields magnitude is much smaller than the anisotropy fields. This suggests that other effects occur, such as a broad anisotropy field distribution and/or slightly canted magnetization.

3. Multilayered FE (1 1 0)/MO (1 1 0) atomic step decoration

Ultrathin Fe deposits on W (1 1 0) [13], and to a less extent on Mo (1 1 0) [14,15], have been much studied as a

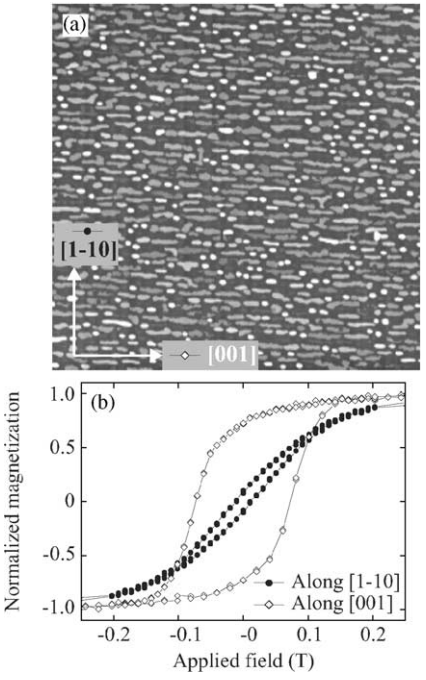

Fig. 4. (a) Ex situ $10 \times 10\,\mu m$ AFM image of Fe/Mo (1 1 0) step-decorated stripes. (b) Room temperature VSM in-plane hysteresis loops of the stripes.

model system due to perfect wetting of the Fe monolayer and absence of intermixing. For high thickness randomly distributed three-dimensional (3D) Fe islands are known to grow on top of the monolayer at high temperature [16,17], whereas the fabrication of continuous films requires moderate temperature or temperature-gradient deposition [18,17]. By following a suitable mixture of the two procedures, we could produce nanometer-thick self-organized Fe(1 1 0)/Mo(1 1 0) structures, as reported below.

Our deposition technique in this case is pulsed laser deposition, performed under UHV on a flat and perfectly single crystalline 10 nm thick Mo (1 1 0) buffer layer on $Al_2O_3(1\,1\,\bar{2}\,0)$ [16]. Fig. 4a shows an ex situ AFM image after deposition of a nominal thickness of 2 nm Fe at 425 K and subsequent 1 h annealing at 725 K, resulting in stripe-shaped Fe dots with a mean height of 6 nm. A close examination of Fig. 4a and comparison with in situ STM images reveal that the stripes are parallel to the atomic steps of the Mo (1 1 0) surface, each step being decorated by one chain of stripes. The period ($\sim$200 nm) and stripe direction ($\sim$[0 0 1]) of the array are directly related to the slight miscut of the Al_2O_3 substrate, estimated at 0.05° along [1 $\bar{1}$ 0]. The mechanisms underlying the growth of rather thick stripes in a self-organized step-decoration fashion lies outside the scope of this paper, and will be reported elsewhere.

On this wafer, shape and magnetocrystalline anisotropy [15] both favor magnetization alignment along [0 0 1], as confirmed by vibrating sample magnetometry hysteresis loops (see Fig. 4b). The high remanence along [0 0 1] at 300 K is a direct consequence of the vertical growth of the wires, and thus of their large volume. This contrasts with conventional step decorated ultra-flat stripes grown in the monolayer range, that may even not be ferromagnetic at 300 K [1].

We acknowledge helpful discussions with M. El Hajal (CNRS) and G. Tatara (Osaka) about the imaginary error function. We are also grateful to Ph. David (CNRS), V. Santonacci (CNRS) and G.Kroder (MPI) for technical support.

References

[1] J. Hauschild, U. Gradmann, H.J. Elmers, Appl. Phys. Lett. 72 (24) (1998) 3211.
[2] A. Dallmeyer, C. Carbone, W. Eberhardt, C. Pampuch, O. Rader, W. Gudat, P. Gambardella, K. Kern, Phys. Rev. B 61 (8) (2000) R5133.
[3] K. Bromann, M. Giovannini, H. Brune, K. Kern, Euro. Phys. J. D 9 (1999) 25.
[4] A. Bourret, Surf. Sci. 432 (1999) 37.
[5] H. Takeshita, Y. Suzuki, H. Akinaga, W. Mizutani, K. Ando, T. Takayama, A. Itoh, K. Tanaka, J. Magn. Magn. Mater. 165 (1997) 38.
[6] S.L. Silva, C.R. Jenkins, S.M. York, F. Leibsle, Appl. Phys. Lett. 76 (9) (2000) 1128.
[7] B. Voigtländer, G. Meyer, N.M. Amer, Phys. Rev. B 44 (18) (1991) 10354.
[8] D.D. Chambliss, R.J. Wilson, S. Chiang, Phys. Rev. Lett. 66 (13) (1991) 1721.
[9] B. Voigtländer, G. Meyer, N.M. Amer, Surf. Sci. Lett. 255 (1991) L529.
[10] O. Fruchart, M. Klaua, J. Barthel, J. Kirschner, Phys. Rev. Lett. 83 (14) (1999) 2769.
[11] O. Fruchart, M. Klaua, J. Barthel, J. Kirschner, Appl. Surf. Sci. 162–163 (2000) 529.
[12] R.W. Chantrell, N.Y. Ayoub, J. Popplewell, J. Magn. Magn. Mater. 53 (1985) 199.
[13] U. Gradmann, Magnetism in ultrathin transition metal films, in: K. Buschow (Ed.), Handbook of magnetic materials, Vol. 7, Elsevier Science Publishers, North-Holland, 1993, pp. 1–96.
[14] J. Malzbender, M. Przybylski, J. Giergiel, J. Kirschner, Surf. Sci. 414 (1998) 187.
[15] O. Fruchart, J.-P. Nozières, D. Givord, J. Magn. Magn. Mater. 207 (1999) 158.
[16] P. Jubert, O. Fruchart, C. Meyer, Phys. Rev. B 64 (2001) 115419.
[17] H. Bethge, D. Heuer, C. Jensen, K. Reshöft, U. Köhler, Surf. Sci. 331–333 (1995) 878.
[18] H.J. Elmers, U. Gradmann, Appl.Phys. A 51 (1990) 255.